Kinetics of the Reactions of the *Escherichia coli* Molecular Chaperone DnaK with ATP: Evidence That a Three-Step Reaction Precedes ATP Hydrolysis†

Sergey V. Slepenkov and Stephan N. Witt*

Department of Biochemistry and Molecular Biology, Louisiana State University Medical Center, 1501 Kings Highway, Shreveport, Louisiana 71130-3932

Received August 19, 1997; Revised Manuscript Received November 18, 1997

ABSTRACT: The mechanism of the ATPase cycle of the 70-kDa *Escherichia coli* molecular chaperone DnaK was investigated by following ATP-induced changes in the tryptophan fluorescence of DnaK. Three steps in the cycle were investigated. (i) Stopped-flow experiments revealed that ATP induces a biphasic reduction in the tryptophan fluorescence of DnaK. The rate of the fast fluorescence transition exhibited a hyperbolic dependence on the ATP concentration, with a maximum rate equal to 56 (± 10) s^{-1} at 35 °C, whereas the rate of the slow fluorescence transition was nearly independent of the ATP concentration (4.2 ± 0.2 s^{-1}). These results are consistent with the three-step sequential reaction E + ATP ⇔ E−ATP ⇔ E*−ATP ⇔ E**−ATP prior to DnaK-catalyzed ATP hydrolysis, where the formation of a collisional complex (E−ATP) causes no change in fluorescence but is followed by two first-order transitions that reduce the fluorescence. (ii) The kinetics of ADP replacement from preformed DnaK−ADP complexes by ATP followed simple exponential kinetics, k_{ADP} = 0.038 (± 0.002) s^{-1} at 35 °C. The ADP off rate was reduced ∼ 10-fold by inorganic phosphate (20 mM). (iii) Single-turnover experiments ([DnaK] = [ATP] = 1 μM) revealed a slow, first-order increase in tryptophan fluorescence [k_{obs} = 0.0015 (± 0.0001) s^{-1}, 37 °C] that was identical to the rate of DnaK-catalyzed ATP hydrolysis [k_{hy} = 0.0014 (± 0.0001) s^{-1}, 37 °C]. This slow increase in fluorescence is consistent with a E** → E conformational transition. A model for the ATPase cycle of DnaK is proposed in which ATP has two distinct functions: ATP binding to the ATPase domain triggers two conformational transitions in a chaperone molecule, and ATP hydrolysis—the slow step in the reaction cycle—reverses the transitions.

Molecular chaperones are a highly conserved family of proteins that function to promote a variety of cellular processes that are essential for life, such as the folding, transport, and assembly of other proteins. They are usually categorized according to their molecular weight and range in size from 10 to 100 kDa. The 70-kDa family of molecular chaperones are K^+-dependent, mechanochemical ATPases (*1*−*3*) that carry out the above functions via a unique mechanism whereby an individual chaperone molecule discriminates between folded and partially unfolded segments of another protein and selectively binds to the latter (for reviews see refs *4*−*6*). The binding and hydrolysis of ATP by these chaperones is tightly coupled to the binding and release of substrates. The mechanism of how a chaperone utilizes free energy from ATP binding and hydrolysis to alter its structure and hence modulate its activity with (poly)-peptides is of great interest.

The 70-kDa molecular chaperones are composed of two functional domains: ATP binding and hydrolysis occurs in the 44-kDa NH_2-terminal domain, and selective substrate binding occurs in the 23-kDa COOH-terminal domain. The three-dimensional structures of the separate domains have been determined (*7*−*9*).

There is considerable evidence that 70-kDa molecular chaperones are molecular switches, turned on and off by its interactions with ATP. For example, (i) recent reports have indicated that ATP binding, rather than hydrolysis, alters the affinity of peptides for the chaperone substrate binding domain (*2*, *10*, *11*); (ii) solution small-angle X-ray scattering experiments have revealed two distinct conformations of the 70-kDa chaperone DnaK, and ATP induces the conversion of one conformation to the other (*12*, *13*); (iii) the ATP-induced conformational change results in a reduction in tryptophan fluorescence and a blue shift of the fluorescence maximum (*14*−*16*); and (iv) ATP induces changes in the protease digestion pattern of 70-kDa chaperones (*17*−*19*). An ideal way to investigate the coupling of ATP binding to changes in the conformational state of the chaperone is to follow the ATP-induced changes in tryptophan fluorescence in real time (*16*, *20*, *21*).

In this study, the pre-steady-state kinetics of the reactions between ATP and DnaK were investigated over a range of temperatures (15−37 °C) using stopped-flow fluorescence in order to determine both the reaction mechanism and the activation energy barriers for the reaction steps, where possible. Evidence is presented herein for a three-step sequential reaction prior to DnaK-catalyzed ATP hydrolysis. The rate-determining step in the reaction between DnaK and ATP under single-turnover conditions is ATP hydrolysis.

†Support for this work came from the NIH (GM51521) and an American Cancer Society Junior Faculty Research Award (JFRA-583).

* To whom correspondence should be addressed: Tel (318) 675-7891; FAX (318) 675-5180; E-mail SWITT1@LSUMC.EDU.

S0006-2960(97)02048-5 CCC: $15.00
Published on Web 01/09/1998

MATERIALS AND METHODS

Protein. All reagents were of the highest purity and were purchased from Sigma, unless stated otherwise. The protein was isolated as previously described (*22*) and stored at 4 °C in a HEPES[1] sample buffer (25 mM HEPES/50 mM KCl/5 mM $MgCl_2$/5 mM 2-mercaptoethanol at pH = 7.0). After the last purification step (Mono Q column), Mono Q column fractions were dialyzed for 4 days against 16 L of sample buffer (4 L/day) at 4 °C. SDS−PAGE of purified DnaK revealed one band at 70 ± 1 kDa, and densitometric scans of the gel showed that the protein was >95% pure. Protein concentration was determined by the Bio-Rad protein assay according to the manufacturer's instructions and verified by an absorbance determination using the extinction coefficient $\epsilon_{280} = 15.8 \times 10^3\ M^{-1}\ cm^{-1}$ (*23*). No corrections were made for the slight variation of the pH of the HEPES sample buffer over the temperature range (15−37 °C) at which samples were incubated.

The endogenous nucleotide content in DnaK preparations was estimated by the A_{280}/A_{260} ratio. In every case, $A_{280}/A_{260} > 1.5$, which indicated that DnaK was nucleotide-free (*24*). Nevertheless, to verify this result DnaK was subjected to acid precipitation in order to liberate any endogenous nucleotide, and then the supernatant was analyzed using HPLC. Briefly, DnaK (60 μM) was incubated with 0.5 M $HClO_4$ for 15 min at 4°C, and then the denatured protein was separated by centrifugation (10000*g* for 20 min, 4 °C). The supernatant was then neutralized with 5 M KOH on ice, centrifuged once more at 4 °C, and lyophilized. The lyophilized material was then dissolved in HPLC column buffer (0.05 M potassium phosphate, pH = 7.0). Control samples consisted of (i) a solution of ADP with no protein and (ii) a solution of DnaK with added ADP. These controls were subjected to the same acid treatment as described above. Samples treated in the above manner were then analyzed using a C_{18} column (218TP1010, Vydac, Hesperia, CA) with UV detection (λ = 254 nm). Using this method, as little as 250 pmol of ADP could be detected. On the basis of this HPLC analysis, we conclude that our DnaK preparations were 94% nucleotide-free; that is, up to 6% of the molecules contained ADP.

The effect of inorganic phosphate on the kinetics of ADP dissociation from preformed DnaK−ADP complexes was examined at 25 °C using either a stopped-flow instrument or a steady-state fluorescence spectrometer in the time base mode (see below). Inorganic phosphate (0.25−30 mM) was introduced into samples of preformed DnaK−ADP complexes by the addition of a small aliquot of a concentrated stock solution of KH_2PO_4/K_2HPO_4 (pH = 7.0). To control for the possible effect of K^+ ions and the ionic strength on the ADP off rate, in a separate experiment the concentration of the K^+ ion was increased from 50 to 120 mM. This 2.4-fold increase in the K^+ ion concentration had no effect on the ADP off rate.

Instrumentation. An Applied Photophysics Ltd. (Leatherhead, U.K.) stopped-flow spectrometer (SX-17MV) with fluorescence detection was used to follow both the rapid binding of ATP to DnaK and the dissociation of ADP from preformed DnaK−ADP complexes. The instrument dead time was 1.6 ms. Light from a 150 W xenon lamp went through an excitation monochromator and then into the observation cell via an optical fiber light guide. For the experiments described in this report, λ_{ex} = 290 or 295 nm (2.5 nm bandwidth). Fluorescence emission was collected using a photomultiplier tube that was mounted at 90° to the incident light. An Oriel long-pass filter with cutoff wavelength of 335 nm was used to eliminate stray excitation radiation. The path length of the observation cell was 2 mm. The instrumental time constant was equal to 0.5% the half-time of the fastest phase. Samples were degassed prior to loading into the stopped-flow syringes. One syringe contained DnaK; the other, Mg-ATP. Temperature control of both the jacketed reactants and the jacketed mixing chamber was achieved with a circulating external water bath ($T = \pm$ 0.1 °C). Stopped-flow traces are the average of 7−10 individual traces. In some cases, data were collected using a split time base mode.

A Photon Technology Inc. (South Brunswick, NJ) StrobeMaster lifetime spectrometer with a SE-900 steady-state fluorescence option was used to monitor nucleotide-induced changes in tryptophan fluorescence in several experiments. The excitation source was a 75 W xenon arc lamp, and the detection was accomplished with a photon counting detector (PTI Model 710). (i) To obtain fluorescence emission spectra of DnaK with nucleotides, DnaK was incubated with added nucleotide at 25 °C for 10 min prior to the start of the emission scan. The excitation wavelength was either 290 or 295 nm (3 nm bandwidth); the emission bandwidth was 5 nm. (ii) The dissociation of ADP from preformed DnaK−ADP complexes was monitored by following the decrease in fluorescence upon the addition of excess ATP. For these experiments the instrument was used in the time base mode, with λ_{ex} = 295 nm (3 nm bandwidth) and λ_{em} = 340 nm (5 nm bandwidth). (iii) The slow increase in tryptophan fluorescence in the single-turnover experiments was also monitored using the fluorescence spectrometer in the time base mode, with λ_{ex} = 295 nm (3 nm bandwidth) and λ_{em} = 340 nm (5 nm bandwidth). In all experiments, samples were maintained in a quartz cuvette (1 cm path length) with constant stirring and temperature control via an external circulating heating/cooling bath ($\Delta T = \pm 0.2$ °C). Sample temperature was verified using a hand-held thermocouple that was placed directly into the sample.

Curve Fitting/Data Analysis. The stopped-flow traces representing ATP binding to DnaK were analyzed using a curve-fitting program that used a Marquardt algorithm based on the program Curfit given in Bevington (*25*). All stopped-flow traces were fit to both a single-exponential function ($F(t) = \Delta F_\alpha\ e^{-k_\alpha t} + \gamma$) and a double-exponential function ($F(t) = \Delta F_\alpha\ e^{-k_\alpha t} + \Delta F_\beta\ e^{-k_\beta t} + \gamma$) and then the residuals from both fits were compared. In some cases, data were fit to a triple-exponential function. The terms $\Delta F_{\alpha,\beta}$, $k_{\alpha,\beta}$, and γ represent amplitudes, rate parameters, and the floating end point, respectively. It should be noted that the rate parameters k_α and k_β are not individual rate constants; they are functions of several rate constants.

The program KaleidaGraph (Synergy Software, Reading, PA) was used to fit kinetic curves obtained from experiments that probed ADP dissociation from preformed DnaK−ADP

[1] Abbreviations: HEPES, *N*-(2-hydroxyethyl)piperazine-*N*′-2-ethanesulfonic acid; HPLC, high-performance liquid chromatography; hsc70, 70-kDa heat shock cognate protein; SDS−PAGE, sodium dodecyl sulfate−polyacrylamide gel electrophoresis.

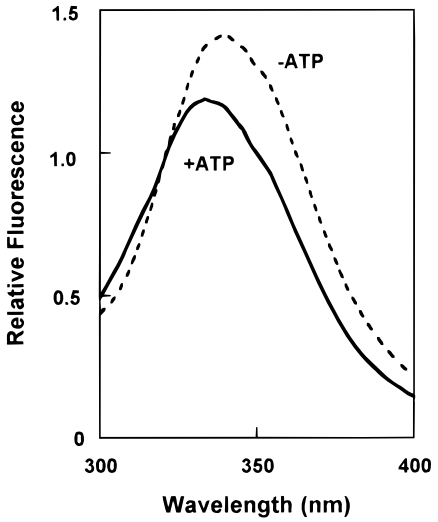

FIGURE 1: Effect of ATP on the fluorescence spectrum of DnaK. Fluorescence emission spectra of DnaK with and without ATP are shown. Conditions: [DnaK] = 1.0 μM; [ATP] = 1.0 mM. Temperature = 25 °C. λ_{ex} = 295 nm; excitation bandwidth = 3.0 nm; emission bandwidth = 5 nm.

complexes to a single-exponential function and to analyze the plot of $1/k_{obs}$ vs $[P_i]$. In addition, KaleidaGraph was also used to fit the single-turnover fluorescence data to a single-exponential function and to a function given in the text. Arrhenius plots were analyzed and the uncertainties in the activation parameters were determined using the program Scientist (MicroMath, Salt Lake City, UT).

RESULTS

Effect of ATP on the Fluorescence Spectrum of DnaK. DnaK, which possesses a single tryptophan residue (located at position 102 in the ATP binding domain) (*26*), exhibited a steady-state fluorescence spectrum centered at λ_{max} = 340 nm in the absence of nucleotide at 25 °C (Figure 1). The addition of ATP (1.0 mM) resulted in a rapid 14% reduction in fluorescence and a 5-nm blue shift of λ_{max}. In contrast, ADP (1.0 mM) had no effect on the fluorescence of DnaK within 3−4 min after addition at 25 °C but caused a ≈ 7% increase in fluorescence after approximately 90 min (data not shown).

Kinetics of the Rapid ATP-Induced Reduction in the Tryptophan Fluorescence of DnaK. The rapid, ATP-induced reduction in tryptophan fluorescence was monitored by mixing equal volumes of ATP and DnaK using a stopped-flow fluorescence instrument. In all experiments, the concentration of ATP was varied (1−2000 μM) at a fixed concentration of DnaK (1.0 μM) over the range 15−35 °C. Representative stopped-flow data, acquired at 25 °C with a time base of 10 s, are shown in Figure 2. Plots of the residuals from fits of the data to both single- and double-exponential functions are shown beneath the data in Figure 2. Over the range of temperatures, as the ATP concentration was increased the stopped-flow traces became increasingly biphasic. For example, the traces acquired with [ATP] = 10 μM were reasonably well fit by a single-exponential

$$F(\mathbf{t}) = [0.213(\pm 0.001)] \exp[-0.71(\pm 0.01)\mathbf{t}] - 0.224(\pm 0.001) \quad (1)$$

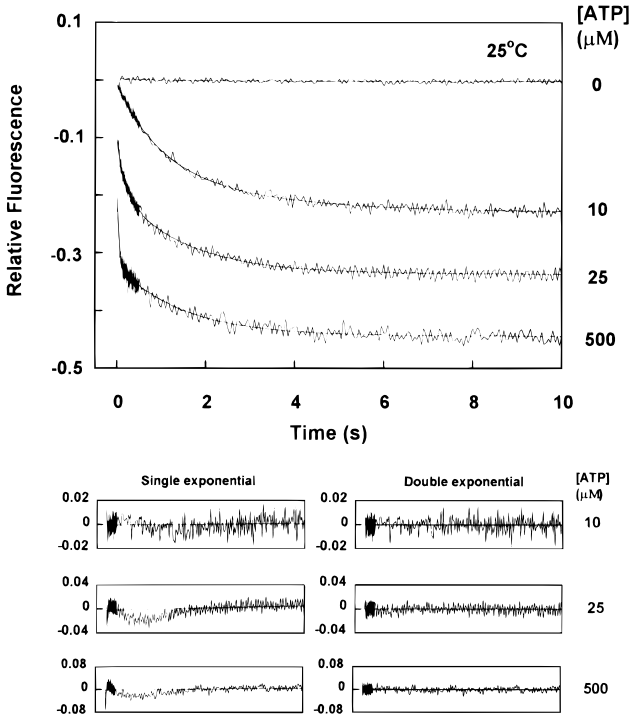

FIGURE 2: Kinetics of the rapid ATP-induced changes in the tryptophan fluorescence of DnaK. The pre-steady-state reaction between DnaK and ATP were followed using stopped-flow fluorescence. Solid lines are the best fits of the stopped-flow data to the double-exponential function $F(t) = \Delta F_\alpha e^{-k_\alpha t} + \Delta F_\beta e^{-k_\beta t} + \gamma$. Residuals for fits to both a single- and a double-exponential function are shown beneath the kinetic traces. Traces were obtained in a split time base mode where 200 points were collected in the first 0.5 s and 200 points were collected over the next 10 s. The best-fit rate parameters, determined from a double-exponential fit, were for [ATP] = 10 μM, k_α = 1.0 (± 0.1) s^{-1}, and k_β = 0.34 (±0.10) s^{-1}; [ATP] = 25 μM, k_α = 5.5 (±0.6) s^{-1}, and k_β = 0.66 (±0.03) s^{-1}; and [ATP] = 500 μM, k_α = 19.7 (±1.3) s^{-1}, and k_β = 0.67 (±0.03) s^{-1}. Conditions: [DnaK] = 1.0 μM; [Mg-ATP] = 0, 10, 25, or 500 μM; temperature = 25 °C; λ_{ex} = 290 nm (bandwidth = 2.3 nm); 335 nm long-pass filter.

where the rate of the transition was 0.71 (± 0.01) s^{-1}. There was some improvement in the fit, as expected, when a double-exponential was used (see residuals). The biphasic reduction in fluorescence was pronounced when [ATP] ≥ 100 μM. For example, when [ATP] = 500 μM, 50% of the total reduction in fluorescence occurred with a half-time ($t_{1/2}$) of approximately 30 ms ($t_{1/2}$ = ln 2/20 s^{-1}), and 50% of the total reduction in fluorescence occurred with a half-time of approximately 1 s ($t_{1/2}$ = ln 2/0.67 s^{-1}). The traces acquired at 500 μM ATP followed

$$F(\mathbf{t}) = [0.125(\pm 0.005)] \exp[-19.7(\pm 1.3)\mathbf{t}] + [0.122(\pm 0.002)] \exp[-0.67(\pm 0.03)\mathbf{t}] - 0.441(\pm 0.002) \quad (2)$$

where the rates of the fast and slow transitions were 19.7 (± 1.3) s^{-1} and 0.67 (± 0.03) s^{-1}, respectively. Biphasic kinetics were also observed in the rapid mixing experiments conducted at 15 and 35 °C. In our experiments, values for k_α and k_β have 10−20% error and 3−6% error, respectively. Since the steady-state rate of DnaK-catalyzed ATP hydrolysis at 25 °C (k_{hy} < 0.001 s^{-1}) (*22*, *27*, *28*) is more than 2 orders of magnitude less than k_β (0.67 s^{-1}) and more than 4 orders of magnitude less than k_α (19.7 s^{-1}), we conclude that these

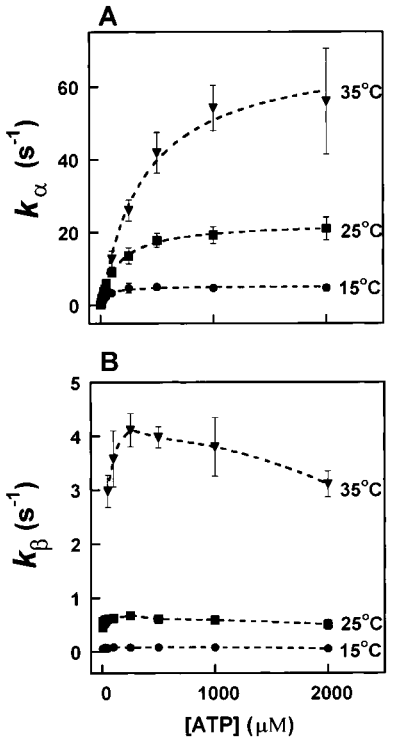

FIGURE 3: Plots of the apparent rate constants (k_α and k_β) versus [ATP]. k_α and k_β values were obtained from fits of the stopped-flow traces to a double-exponential function (see legend to Figure 2). (A) k_α versus [ATP]. (B) k_β versus [ATP]. Each data point represents the average of two or three experiments, which were conducted on different days with different preparations of DnaK. Error bars represent two times the average deviation. The dotted lines through each data set is to help guide the eye.

two first-order fluorescence transitions result from two different ATP-induced conformational transitions in a molecule of DnaK.

In addition to monitoring the rapid reaction between ATP and DnaK over a 10 s time base, the reaction was also monitored over shorter and longer time bases. Over the short time base (0−0.5 s), the reduction in fluorescence followed single-exponential kinetics, and the rate constant was similar within experimental error to the rate constant for the fast fluorescence transition (k_α) of the data acquired over 10 s (Figure 2). Over the long time base (0−100 s), three fluorescence transitions were observed. The amplitude of the third transition was approximately 10% of the total amplitude at 25 °C. The rate of the third fluorescence transition was approximately 0.03−0.05 s^{-1} and was independent of the ATP concentration. Because the rate of this slow, third fluorescence transition was very close to the rate of ADP dissociation from DnaK (see below), the third fluorescence transition is probably due to the replacement of the small amount of endogenous ADP by ATP.

To rule out the possibility that the rapid reduction in tryptophan fluorescence at high ATP concentrations was due to an inner filter effect, experiments were also conducted using an excitation wavelength of 295 nm, a wavelength where ATP has no appreciable absorbance. With 295 nm excitation, the same results were obtained as those shown in Figure 2; therefore the rapid phase of quenching is not due to an inner filter effect.

In Figure 3A, the rate of the fast fluorescence transition, k_α, is plotted versus [ATP]. At each temperature, k_α exhibited a hyperbolic dependence on the concentration of ATP, with a maximum rate of 5.0 ± 0.7 s^{-1}, 18.7 ± 1.1 s^{-1}, and 56 ± 10 s^{-1} at 15, 25, and 35 °C, respectively. In Figure 3B, the rate of the slow fluorescence transition, k_β, is plotted versus [ATP]. Over a wide range of ATP concentrations, k_β values at 15 and 25 °C exhibited no appreciable dependence on the concentration of ATP, whereas the plot of k_β(35 °C) showed a slight increase in the rate (from 0 to 200 μM ATP) and then a slight decrease in the rate (from 1000 to 2000 μM). The maximum rate of the slow transition was 0.085 (± 0.005) s^{-1}, 0.67 (± 0.02) s^{-1}, and 4.2 (± 0.2) s^{-1} at 15, 25, and 35 °C, respectively.

Scheme 1

$$\mathrm{ATP + E} \overset{K_1}{\Leftrightarrow} \mathrm{E{-}ATP} \underset{k_{-2}}{\overset{k_2}{\Leftrightarrow}} \mathrm{E^*{-}ATP} \underset{k_{-3}}{\overset{k_3}{\Leftrightarrow}} \mathrm{E^{**}{-}ATP}$$

The biphasic kinetics and the hyperbolic dependence of k_α on the ATP concentration are consistent with the three-step sequential mechanism shown in Scheme 1. The asterisks denote states with reduced fluorescence relative to the E state, the monomeric chaperone molecule. In the first step, a bimolecular reaction between a molecule of DnaK and a molecule of ATP produces a collisional complex (E−ATP) with no change in fluorescence. In the second step, the collisional complex triggers a conformational transition that yields a transient with reduced fluorescence (E*−ATP). In the third step, a slower conformational transition occurs, yielding another transient with reduced fluorescence (E**−ATP). The fluorescence of the four DnaK species is F(E) ≈ F(E−ATP) > F(E*−ATP) > F(E**−ATP). Such a mechanism leads to monophasic kinetics at low concentrations of ATP and biphasic kinetics at large concentrations of ATP. The maximum rate of E*−ATP complex formation ($k_2 + k_{-2}$) is approximated by the asymptote of the plot of k_α versus [ATP]. Similarly, the maximum rate of E**−ATP complex formation ($k_3 + k_{-3}$) is approximated by the asymptote of the plot of k_β versus [ATP]. The apparent second-order rate constant (k^a) for ATP binding to DnaK is defined by the slope of the plot of k_α vs [ATP] in the limit of [ATP] → 0 (Figure 3A), and $k^a \approx K_1 k_2$ (*29*). In addition, the ATP concentration where k_α equals half the maximum rate approximates the equilibrium association constant for the initial step (K_1, M^{-1}). The various parameters from the $k_{\alpha,\beta}$ vs [ATP] plots are given in Table 1. Scheme 1 is not the only mechanism that can account for the observed biphasic kinetics of ATP binding to DnaK; another possible mechanism is discussed below.

Kinetics of ADP Dissociation from Preformed DnaK−ADP Complexes. The kinetics of ADP dissociation from preformed DnaK−ADP complexes were investigated using stopped-flow fluorescence. One syringe contained a large excess of ATP (1.0 mM); the other, ADP (5 μM) and DnaK (2 μM). Due to the tight binding of ADP to DnaK (K_d ∼ 100 nM) (*21*), the syringe with DnaK and ADP contained a homogeneous population of preformed DnaK−ADP complexes. When these complexes are mixed with a large excess of ATP, ADP dissociates and is rapidly replaced by ATP

$$\mathrm{E{-}ADP} \xrightarrow{k_{ADP}} \mathrm{E + ADP} \xrightarrow{[ATP]} \mathrm{E^{**}{-}ATP} \qquad [ATP] \gg [E{-}ADP] \quad (3)$$

Table 1: Kinetic Constants from the Pre-Steady-State Experiments (Figures 2 and 3)

	kinetic constant			
temperature (°C)	k^{a} [a] (M^{-1} s^{-1})	K_1 [b] (M^{-1})	$k_2 + k_{-2}$ [c] (s^{-1})	$k_3 + k_{-3}$ [d] (s^{-1})
15	$5.6\ (\pm0.3) \times 10^4$ ($n = 2$)	$2.3\ (\pm0.9) \times 10^4$ ($n = 2$)	$5.0\ (\pm0.7) \times 10^0$ ($n = 2$)	$8.5\ (\pm0.5) \times 10^{-2}$ ($n = 2$)
25	$9.0\ (\pm0.7) \times 10^4$ ($n = 3$)	$9.8\ (\pm1.6) \times 10^3$ ($n = 3$)	$1.9\ (\pm0.1) \times 10^1$ ($n = 3$)	$6.7\ (\pm0.2) \times 10^{-1}$ ($n = 3$)
35	$1.2\ (\pm0.2) \times 10^5$ ($n = 2$)	$3.7\ (\pm0.6) \times 10^3$ ($n = 2$)	$5.6\ (\pm1.0) \times 10^1$ ($n = 2$)	$4.2\ (\pm0.1) \times 10^0$ ($n = 2$)

[a] Slope of k_α vs [ATP] plots in the limit of [ATP] → 0 (Figure 3A). [b] Reciprocal ATP concentration where k_α equals half the maximum rate (Figure 3A). [c] Asymptote of k_α vs [ATP] plots (Figure 3A). [d] Asymptote of k_β vs [ATP] plots (Figure 3B).

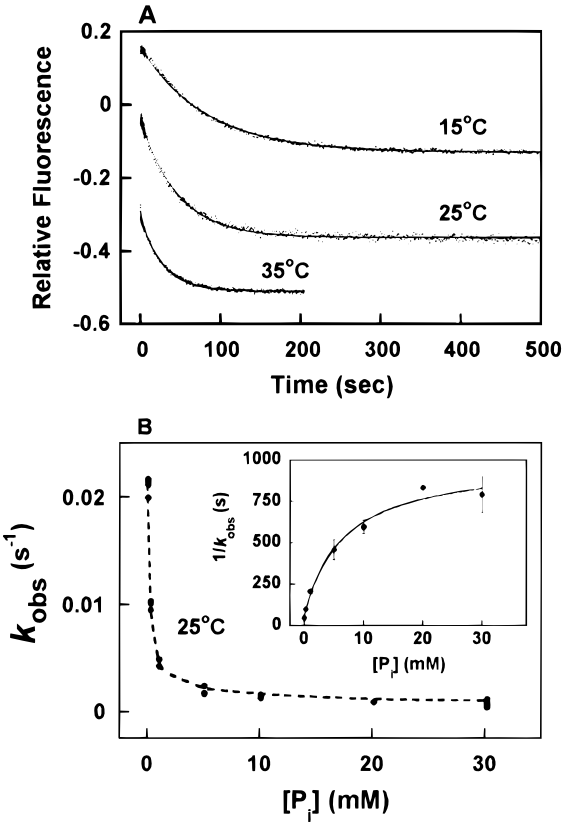

FIGURE 4: Kinetics of ADP dissociation from preformed DnaK−ADP complexes. (A) The kinetics of Mg-ADP dissociation from DnaK were probed by the rapid mixing of equal volumes of DnaK−ADP complexes and Mg-ATP, such that the concentrations of reactants upon mixing were [DnaK−Mg-ADP] = 2 μM, [Mg-ADP] = 3 μM, and [Mg-ATP] = 1.0 mM. Stopped-flow traces (dotted lines) were fitted to the equation $F(t) = \Delta F \exp(-k_{ADP}\, t) + \gamma$ (solid lines). The best-fit rate constants were as follows: at 15 °C, k_{ADP} = 0.012 (±0.001) s^{-1}; at 25 °C, k_{ADP} = 0.022 (±0.001) s^{-1}; and at 35 °C, k_{ADP} = 0.036 (±0.002) s^{-1}. Dashed lines are to help guide the eye. (B) Dissociation experiments were conducted by varying the concentration of P_i at 25 °C. Fits to a single-exponential gave values for the observed rate constant for ADP dissociation (k_{obs}), and then the reciprocal of the observed rate constant ($1/k_{obs}$) was plotted versus [P_i]. The data were fit to the equation $1/k_{obs} = \{K_d(P_i) + [P_i]\}/\{k_{ADP}K_d(P_i) + k^*_{ADP}\,[P_i]\}$ (solid line), yielding $K_d(P_i)$ = 0.40 (±0.26) mM, k_{ADP} = 0.016 (±0.001) s^{-1}, and k^*_{ADP} = 0.0010 (±0.0001) s^{-1}. Instrumental conditions were the same as in the legend to Figure 2. Temperature = 15, 25, and 35 °C.

which reduces the tryptophan fluorescence of DnaK, as shown in Figure 4A. Since the reactions depicted in Figure 4A are much slower than ATP binding to DnaK (compare to Figure 2), we reasonably conclude that the traces reflect ADP dissociation from preformed DnaK−ADP complexes. The dissociation traces followed single-exponential kinetics [$F(t) = \Delta F e^{-k_{ADP}t} + \gamma$], and k_{ADP} varied from 0.01 to 0.04 s^{-1} between 15 and 35 °C (Table 2).

Table 2: Effect of P_i on the Rate of ADP Dissociation from DnaK

temperature (°C)	k_{ADP} (s^{-1}) (P_i = 0 mM)	k^*_{ADP} (s^{-1}) (P_i = 20 mM)
15	$1.2\ (\pm0.1) \times 10^{-2}$ ($n = 3$)	$6.4\ (\pm0.8) \times 10^{-4}$ ($n = 2$)
25	$2.2\ (\pm0.1) \times 10^{-2}$ ($n = 4$)	$1.4\ (\pm0.2) \times 10^{-3}$ ($n = 2$)
35	$3.8\ (\pm0.2) \times 10^{-2}$ ($n = 3$)	$3.2\ (\pm0.2) \times 10^{-3}$ ($n = 5$)

Several studies have shown that inorganic phosphate (P_i)—a product of the hydrolysis of ATP—inhibits the dissociation of ADP from preformed chaperone−ADP complexes (*16, 21, 30, 31*). Because such product inhibition may be important biologically, we investigated the effect of P_i on the ADP off rate from preformed DnaK−ADP complexes. Samples were prepared as described above, and then P_i (KH_2PO_4/K_2HPO_4, pH = 7.0) was added from a concentrated stock solution to give a final concentration between 0.25 and 30 mM. Kinetic traces were fit to a single-exponential function to determine values for the observed first-order rate constant (k_{obs}) for ADP dissociation. At 25 °C, k_{obs} decreased from 0.022 to 0.005 s^{-1} between 0 and 1.0 mM P_i and then decreased further to an asymptotic value of ∼0.001 s^{-1} for [P_i] ≥ 20 mM (Figure 4B). There was approximately a 10% error associated with these ADP off kinetic traces. Since DnaK is a K^+-dependent ATPase, and because the K^+ ion concentration also increased upon the addition of P_i, we also checked to see whether an increase in the K^+ ion concentration affected the ADP off rate. When the K^+ ion concentration was increased from 50 to 120 mM (by adding KCl), there was no change in the off rate, demonstrating that P_i and not K^+ inhibits ADP dissociation from preformed DnaK−ADP complexes.

The plot of $1/k_{obs}$ vs [P_i] (Figure 4B, inset) can be used to distinguish between two different mechanisms for ADP dissociation from DnaK. Scheme 2 shows an ordered release mechanism where P_i binds to an E−ADP complex with an equilibrium dissociation constant defined by $K_d(P_i)$, and P_i dissociation obligatorily precedes ADP dissociation. In this mechanism, the reciprocal of the observed rate constant for the dissociation of ADP is given by eq 4 (see Appendix),

$$\frac{1}{k_{obs}} = \frac{1}{k_{ADP}} + \frac{[P_i]}{k_{ADP}K_d(P_i)} \qquad (4)$$

and in this case, the plot of $1/k_{obs}$ vs [P_i] is a straight line with positive slope. Scheme 3 shows a mixed dissociation

Table 3: Thermodynamic Parameters

	kinetic constant					
thermodynamic parameters	$k^{a\,a}$	$k_2 + k_{-2}$	$k_3 + k_{-3}$	k_{ADP} ([P_i] = 0 mM)	k^*_{ADP} ([P_i] = 20 mM)	$k_{hy}{}^b$
ΔH^* (kcal mol^{-1})	6 (± 1)	21 (± 2)	34.6 (± 0.5)	9.7 (± 0.4)	14.3 (± 0.9)	25.0 (± 0.9)
$\omega \exp(\Delta S^*/R)$ (s^{-1})	$3.2 \times 10^{9 \pm 1}$	$1.4 \times 10^{16 \pm 1}$	$1.5 \times 10^{25.0 \pm 0.4}$	$3.1 \times 10^{5.0 \pm 0.3}$	$4.6 \times 10^{7.0 \pm 0.7}$	$6.4 \times 10^{14.0 \pm 0.7}$
ΔS^* (cal mol^{-1} K^{-1})	−17 (± 5)	16 (± 6)	54.7 (± 1.8)	−35.5 (± 1.3)	−25.4 (± 3.0)	7.2 (± 3.0)

[a] For k^a, the frequency prefactor has units of M^{-1} s^{-1}. [b] The k_{hy} values were determined from the single-turnover experiments. From those experiments we reasonably concluded that $k_{obs} = k_{hy}$.

Scheme 2: Ordered Release

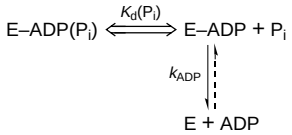

Scheme 3: Mixed Release

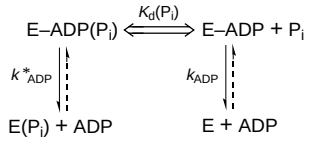

mechanism where P_i binds to an E−ADP complex with an equilibrium dissociation constant defined by $K_d(P_i)$, and ADP dissociates from both E−ADP and E−ADP(P_i) complexes, albeit with different rates. In this mechanism, the reciprocal of the observed rate constant for ADP dissociation is given by eq 5 (see Appendix), and in this case, the plot of $1/k_{obs}$

$$\frac{1}{k_{obs}} = \frac{K_d(P_i) + [P_i]}{k_{ADP}\,K_d(P_i) + k^*_{ADP}[P_i]} \qquad (5)$$

vs [P_i] is a hyperbola. The observed hyperbolic dependence of $1/k_{obs}$ on [P_i] (Figure 4B, inset), therefore rules out the ordered release mechanism and is consistent with the mixed dissociation mechanism (Scheme 3). The fit of the data to eq 5 yielded $K_d(P_i) = 0.40$ (±0.26) mM, $k_{ADP} = 0.016$ (± 0.01) s^{-1}, and $k^*_{ADP} = 0.0010$ (±0.0001) s^{-1}. It should be noted that upon increasing the P_i concentration the amplitude (ΔF) of the kinetic traces did not decrease; such a decrease would be expected if ADP dissociated by the ordered release mechanism. The combined results are consistent with the kinetic mechanism shown in Scheme 3. Values for k^*_{ADP}, determined at 20 mM P_i, over a limited temperature range are given in Table 2. Activation parameters for both k_{ADP} and k^*_{ADP} are given in Table 3.

Single-Turnover Experiments. Single-turnover experiments ([DnaK] = [ATP]) were conducted over a range of temperatures (15−37 °C) using a steady-state fluorescence spectrometer in time base mode. The addition of a stoichiometric amount of ATP to a sample of DnaK produced a rapid reduction in tryptophan fluorescence, and then, over the course of 20−60 min depending on the temperature, the initial reduction in fluorescence was reversed. Since the reduction in fluorescence is due to a E→E** transition, the slow increase in fluorescence is consistent with a E**→E transition. At all temperatures, the portion of each trace that exhibited the slow increase in fluorescence followed single-exponential kinetics, $F(t) = \Delta F(1 - e^{-k_{obs}t}) + \gamma$. Values for k_{obs} were 0.00015 (±0.00001) s^{-1} at 20 °C, 0.00030 (±0.00002) s^{-1} at 25 °C, 0.00050 (±0.00002) s^{-1} at 30 °C, and 0.0015 (±0.0001) s^{-1} at 37 °C. When experiments were conducted with a substoichiometric amount of ATP (0.5 μM ATP/1.0 μM DnaK), the rate did not change. In contrast, when experiments were conducted with a 20% molar excess of ATP (1.2 μM ATP/1.0 μM DnaK), the traces were sigmoidal, with a noticeable lag phase in the early portion of each trace. Controls consisted of monitoring the fluorescence of DnaK without added ATP over the same time scale. Inorganic phosphate (1.0 mM) had no effect on the reaction kinetics shown in Figure 5. Significantly, at 37 °C the rate of DnaK-catalyzed ATP hydrolysis [$k_{hy} = 0.0014$ (±0.0001) s^{-1}] (*22*, *28*) is identical to the rate of the E**→E transition [$k_{obs} = 0.0015$ (± 0.0001) s^{-1}], indicating that ATP hydrolysis is coupled to this transition, as discussed below.

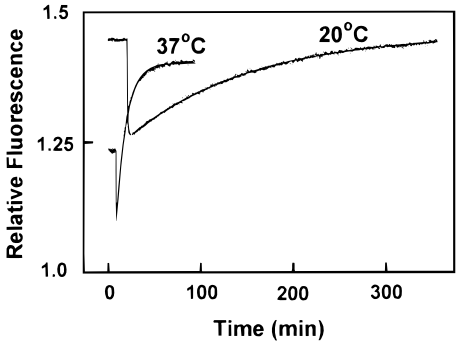

FIGURE 5: Single turnover kinetics. A rapid reduction in fluorescence occurred upon the addition of ATP to DnaK ([ATP] = [DnaK] = 1 μM). The subsequent slow increase in fluorescence corresponds to the E** → E transition. The formation portion of each trace followed the equation $F(t) = \Delta F[1-\exp(-k_{obs}\,t)] + \gamma$ (solid lines), where ΔF, k_{obs}, and γ are the amplitude, the first-order observed rate constant, and the fluorescence at the time zero point, respectively. The best-fit equations were as follows at: 20 °C, $F(t) = 2.3 \times 10^5[1 - \exp(-0.00014t)] + 1.2 \times 10^6$; and 37 °C, $F(t) = 6.6 \times 10^5[1 - \exp(-0.0015t)] + 7.3 \times 10^5$. Since DnaK-catalyzed ATP hydrolysis occurs at the same rate as the slow increase in fluorescence in these single-turnover experiments (see text), we surmise that $k_{obs} \approx k_{hy}$. Conditions: λ_{ex} = 295 nm (bandwidth = 3 nm); λ_{em} = 340 nm (bandwidth = 5 nm).

Temperature Dependence of the Rate Constants. Arrhenius plots (ln k vs $1/T$) were constructed from the data in Tables 1 and 2 (plots not shown). The slope and y-intercept of the plot of ln k versus $1/T$ approximate the activation enthalpy (ΔH^*) and the frequency prefactor [$\omega \exp(\Delta S^*/R)$], respectively. If it is assumed that the frequency factor $\omega = k_B T/h$, where k_B and h are the Boltzmann and Planck constants, then the activation entropy (ΔS^*) can be estimated for each data set from a plot of ln (k/T) vs $1/T$. Activation parameters are given in Table 3. Since nucleotide binds to DnaK and hsc70 with nanomolar equilibrium dissociation constants (*21*, *32*), it is reasonable to assume that $k_2 \gg k_{-2}$

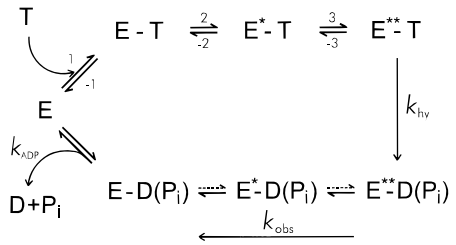

FIGURE 6: Proposed mechanism for the ATPase cycle of 70-kDa molecular chaperones. E, T, D, and P_i represent the chaperone monomer, ATP, ADP, and inorganic phosphate, respectively.

and $k_3 \gg k_{-3}$. Thus, the plot of ln ($k_2 + k_{-2}$) vs $1/T$ gives activation parameters for forward step k_2; the plot of ln($k_3 + k_{-3}$) vs $1/T$ gives activation parameters for forward step k_3.

DISCUSSION

On the basis of the work shown here, we propose a mechanism for the ATPase cycle of DnaK (Figure 6) and discuss it below. Note that the three-step sequential reaction, such as the one we have proposed for ATP binding to DnaK (Scheme 1, Figure 6), has been proposed for other ATP binding proteins, and the analytic solutions to the differential equations associated with such a three-step reaction have been reported (*29*, *33*).

Rapid ATP-Induced Spectral Changes in DnaK. The hyperbolic dependence of k_α—the rate of the fast first-order transition—on the ATP concentration (Figures 2 and 3A) is consistent with the formation of a collisional complex (E−ATP) prior to the first conformational transition (E + ATP ⇔ E−ATP ⇔ E*−ATP) (Figure 6) (*34*). The formation of a collisional complex between DnaK and ATP—without a change in fluorescence—is reasonable since we and others (*20*, *21*) have found that ADP binds to DnaK with no change in fluorescence over the time scale of these experiments. Although the second-order rate constant (k_1) for the formation of a collisional complex cannot be determined from the experiments described here, the apparent association rate constant (k^a) is approximated by the slope of the linear portion of the plot of k_α vs [ATP] (Figure 3A). Between 15 and 35 °C, k^a varied from 5.6×10^4 to 1.2×10^5 M^{-1} s^{-1} (Table 1), which is significantly slower than a diffusion-controlled reaction, 10^8−10^9 M^{-1} s^{-1}. Thus, given the small magnitude of k^a, it might not be the true rate constant for ATP binding to DnaK. We suggest that k^a is smaller than expected because it is composed of two parameters ($k^a \approx K_1 k_2$), and one of them, k_2, is quite small ($k_2 = 20$ s^{-1} at 25 °C).

A comparison of the kinetics of ATP binding to DnaK from this study to the kinetics of ATP binding to hsc70 (*16*) reveals remarkable similarities but also subtle differences. Similar to the results reported here, biphasic changes in tryptophan fluorescence occur upon the rapid binding of ATP to hsc70. The rate of the fast phase increased linearly with increasing [ATP] (up to 550 μM), while the rate of the slow phase was independent of [ATP]. On the basis of those results, it was proposed that ATP binds to hsc70 in the two-step sequential reaction E + ATP ⇔ E*−ATP ⇔ E**−ATP, where collisional complex E*−ATP formation reduces the tryptophan fluorescence. In contrast, in our experiments, the rate of the fast phase, k_α, also increased linearly with increasing [ATP] (up to 250 μM) but deviated from linearity thereafter (Figure 3A). The deviation from linearity led us to propose the three-step sequential mechanism (Scheme 1). Note that at 25 °C the apparent association rate constant for ATP binding to DnaK ($k^a = 9.0 \times 10^4$ M^{-1} s^{-1}) is nearly an order of magnitude smaller than the association rate constant ($k_1 \sim 7 \times 10^5$ M^{-1} s^{-1}) for ATP binding to hsc70. Another interesting difference between DnaK and hsc70, which may relate to the kinetic mechanisms for ATP binding, is that ADP binding does not reduce the fluorescence of DnaK, whereas ADP binding to hsc70 reduces its fluorescence (by 8%). These subtle differences in the ATP binding kinetics and the differential effects of ADP binding on the fluorescence spectra of DnaK and hsc70 reflect subtle differences in the structures of their respective NH_2-terminal domains.

The rapid biphasic reduction in tryptophan fluorescence shown in Figure 2 is distinctly different from the results from a recent study (*21*), which reported a monophasic reduction in tryptophan fluorescence upon mixing DnaK with excess ATP. This difference may be related to the different buffer compositions, pH values, or storage conditions used in the two studies. Note that if the stopped-flow traces in Figure 2 are fitted to a single-exponential function, and the apparent first-order rate constants are plotted versus [ATP], the resultant plot (hyperbola with the asymptote equal to 1.5 s^{-1}) is nearly identical to that reported by Theyssen et al. (*21*).

Scheme 1 is not the only mechanism that can give rise to biphasic kinetics of the type found here. For example, the mechanism in Scheme 4, which includes a preequilibrium between unreactive and reactive forms of DnaK, can also yield biphasic kinetics where the rate of the fast phase of fluorescence change exhibits a hyperbolic dependence on the concentration of ATP. In Scheme 4, subscripts c and o denote states of DnaK in which the ATP binding site is closed and open, respectively. In this mechanism, the fast phase of fluorescence change is due to ATP binding (E_o + ATP ⇔ E_o*−ATP), with $k_2 = 9 \times 10^4$ M^{-1} s^{-1} (at 25 °C), and the deviation of the rate of the fast phase from linearity is due to the rate-limiting preequilibrium (E_c ⇔ E_o), where the sum of the forward and reverse first-order rate constants equals ~20 s^{-1} (at 25 °C). Interestingly, a mechanism with similarities to Scheme 4 has been proposed to account for the cooperative binding of glucose to dimeric yeast hexokinase P-I (*35*). The dual import of hexokinase to this work is that the tertiary structure of the ATP plus glucose binding core of hexokinase is almost identical to the tertiary structure of the ATP-binding core of the N-terminal fragment of Hsc70 (*7*), and hexokinase equilibrates between open and closed conformations in the absence of glucose (*36*). Data from fluorescence temperature-jump experiments that monitored the binding of glucose to dimeric yeast hexokinase P-I were interpreted in terms of a concerted Monod−Wyman−Changeux mechanism, which has isomerization steps similar to the preequilibrium in Scheme 4 (*35*). Thus, because Scheme 4 cannot be ruled out, we cannot definitively assign the phases of fluorescence change to specific reaction steps at this time. On the other hand, because ADP binds to DnaK with no reduction in fluorescence on the time scale of the kinetic experiments, presently we favor Scheme 1, where

collision complex formation between DnaK and ATP also occurs with no reduction in fluorescence.

Scheme 4

$$E_c \overset{K_1}{\leftrightarrow} E_o + ATP \underset{k_{-2}}{\overset{k_2}{\leftrightarrow}} E_o{*}{-}ATP \underset{k_{-3}}{\overset{k_3}{\leftrightarrow}} E_o{**}{-}ATP$$

Adopting the three-step-sequential mechanism in Scheme 1, the biphasic reduction in the tryptophan fluorescence of DnaK in the rapid mixing experiments can be explained by sequential ATP-induced "local" and "global" conformational transitions in a DnaK molecule (see also Figure 6). The rapid conformational transition (E−ATP ⇔ E*−ATP), which occurs with a maximum rate of 20 s^{-1} at 25 °C, probably alters the local environment around the tryptophan residue, which leads to a reduction in tryptophan fluorescence. The values for ΔH^* and ΔS^* of 21 (± 2) kcal mol^{-1} and 16 (± 6) cal mol^{-1} K^{-1}, respectively, are consistent with structural rearrangements during this first conformational transition. We surmise that the slow conformational transition (E*−ATP ⇔ E**−ATP), which occurs with a maximum rate of 0.67 s^{-1} at 25 °C, disrupts interactions that cement together the NH_2-terminal and COOH-terminal domains and also alters the environment around Trp102, which leads to a further reduction in fluorescence. The large values for ΔH^* and ΔS^* of 34.6 (± 0.5) kcal mol^{-1} and 54.7 (± 1.8) cal mol^{-1} K^{-1}, respectively, indicate that substantial structural rearrangements occur during the second conformational transition. Given that the maximum rate (0.67 s^{-1}) and activation enthalpy (34.6 kcal mol^{-1}) for this second conformational transition in DnaK are so similar to the values obtained for the ATP-induced conformational change in hsc70 (0.68 s^{-1} and $\Delta H^* = 40$ kcal mol^{-1}) (*16*), ATP probably induces similar structural changes in hsc70.

Results from two recent studies reinforce our conclusion that ATP binding induces two conformational transitions in a molecule of DnaK. One study (*18*) showed that ATP binding reduced the fluorescence of wild-type DnaK, DnaK163 (a deletion mutant lacking 100 residues from the COOH-terminal domain), and DnaK385 (a deletion mutant lacking most of the COOH-terminal domain) by 14%, 11%, and 5%, respectively. Therefore, 36% (5/14) of the total reduction in fluorescence is due to conformational change in the NH_2-terminal domain, and 64% (9/14) of the total reduction is due to a conformational change in the COOH-terminal domain (or in interactions between the N- and COOH-terminal domains). The other study (*16*) showed that ATP binds to hsc70 with biphasic kinetics, whereas it binds to the 44-kDa ATPase fragment with monophasic kinetics. Both studies indicate that ATP induces two discrete conformational transitions in a 70-kDa chaperone molecule.

Kinetics of ADP Dissociation from Preformed DnaK−ADP Complexes. We have shown that P_i inhibits the dissociation of ADP from DnaK according to Scheme 3. Values for the ADP dissociation rate constant in the absence (k_{ADP}) and presence (k^*_{ADP}) of P_i were determined over a range of temperatures (Table 2). A comparison of the activation parameters for ADP dissociation from DnaK in the presence and absence of P_i (Table 3) gives insight into how P_i inhibits the dissociation of ADP. The presence of inorganic phosphate (20 mM) lead to an increase in both ΔH^* (from 9.7 to 14.3 kcal mol^{-1}) and ΔS^* (from −35.5 to −25.4 cal mol^{-1} K^{-1}) (Table 3), but the increases have opposite effects, however, on the ADP off rate. For example, at 25 °C, the increase in ΔH^* reduced the off rate by a factor of 4.1×10^{-4}, whereas the increase in ΔS^* enhanced the off rate by a factor of 160. Therefore, the observed P_i-induced reduction in ADP off-rate is due to an enthalpic effect. Structural studies on the ATPase domain of hsc70 provide a basis for interpreting how P_i reduces the ADP off rate. The three-dimensional structure of the ATPase domain of hsc70 revealed that Mg^{2+} is octahedrally coordinated in the active site with a β oxygen from ADP, an oxygen atom from P_i, and four H_2O molecules (*37*). Further, the P_i interacts with Lys-71 via a salt bridge and hydrogen bonds to the hydroxyls from two different threonine residues. Assuming a similar Mg^{2+} coordination in the ATPase domain of DnaK, the removal of P_i from the coordination sphere of Mg^{2+}, which would also disrupt the salt bridge and network of hydrogen bonds to surrounding residues, is likely to weaken the bonds between Mg^{2+} and its other ligands. Conversely, the presence of P_i in the coordination sphere of Mg^{2+} should strengthen the interaction between the β oxygen atom of ADP and Mg^{2+}, and thus ADP dissociates more slowly.

The ADP dissociation experiments also revealed that ADP dissociation is not the rate-limiting step in the ATPase cycle. Consider results from experiments conducted at 25 °C (Figures 4 and 5). At 25 °C, k_{ADP} and k^*_{ADP} were 0.022 (± 0.001) s^{-1} and 0.0014 (± 0.0002) s^{-1} (Table 2), respectively; whereas k_{obs}, the apparent rate constant for the slow increase in fluorescence in the single-turnover experiments, equaled 0.0003 (± 0.00002) s^{-1}. Thus, even at high concentrations of inorganic phosphate, the rate-limiting step in the ATPase cycle of DnaK is not ADP dissociation.

We determined the equilibrium dissociation constant for the reaction DnaK−ADP(P_i) ⇔ DnaK−ADP + P_i, $K_d(P_i)$ = 0.40 (± 0.26) mM at 25 °C (Figure 4B). This value is similar to the value [$K_d(P_i) \sim 1$ mM] reported for the dissociation of P_i from hsc70-ADP(P_i) complexes (*32*) but quite different from the value [$K_d(P_i) = 0.45$ μM] reported for the dissociation of P_i from DnaK−ADP(P_i) complexes (*21*). Since our $K_d(P_i)$ value was determined in a very different way than the K_d value of Theyssen and coworkers, possibly the two different constants are for two different reactions.

Single-Turnover Experiments. Experiments in this report demonstrated that the slow increase in fluorescence in the single-turnover experiments occurred at the same rate as ATP hydrolysis. Such a finding can be explained by the two-step sequential mechanism shown in Scheme 5, where hydrolysis precedes the conformational transition, which produces the increase in fluorescence. This mechanism, also referred to as the E** → E transition, has been proposed to account for single-turnover data from experiments conducted on hsc70 and DnaK (*16*, *21*). To test the validity of this mechanism, the kinetic traces in Figure 5 were fit to eq 6

$$F(t) = \Delta F\left(1 - \frac{k_c\, e^{-k_{hy}t} - k_{hy}\, e^{-k_c t}}{k_c - k_{hy}}\right) + \gamma \qquad (6)$$

which governs the formation of E−ADP(P_i) complexes

according to Scheme 5, where k_{hy} and k_c are the first-order rate constants for DnaK-catalyzed ATP hydrolysis and the conformational transition, respectively. The data collected at 20 °C were well fit by eq 6 and yielded k_{hy} and k_c values of 0.00015 (± 0.00001) s^{-1} and 0.0064 (± 0.0019) s^{-1}, respectively. In contrast, fits of the 30 and 37 °C data lead to large errors in k_c, possibly because the term $k_{hy}e^{-k_c t}$ in eq 6 is negligible when $k_{hy} \ll k_c$. However, in this case, eq 6 simplifies to $F(t) = \Delta F(1 - e^{-k_{hy}t}) + \gamma$, consistent with our finding that $k_{obs} = k_{hy}$. Our results are in accord with Scheme 5 where hydrolysis is the rate-limiting step ($k_{hy} \ll k_c$). Previous studies also concluded that hydrolysis is rate-limiting (*21*, *38*). Note that the activation parameters for ATP hydrolysis, deduced from these single-turnover fluorescence experiments, are given in Table 3. Due to the complexity of the chaperone structure, we suggest that two conformational transitions probably occur in the reverse direction [E**−D(P_i) ⇔ E*−D(P_i) ⇔ E−D(P_i)] (Figure 6).

Scheme 5

$$\text{E**}-\text{ATP} \xrightarrow{k_{hy}} \text{E**}-\text{ADP}(P_i) \xrightarrow{k_c} \text{E}-\text{ADP}(P_i)$$

Evidence was presented that ATP binding triggers two conformational transitions in a molecule of DnaK. We proposed that the first conformational transition is local, occurring in the vicinity of Trp102, whereas the second conformational transition is global, affecting the entire chaperone molecule. The intriguing question is, how does this second conformational transition affect the structure of the substrate binding domain? One possibility is that during the second conformational transition the network of hydrogen bonds and/or salt bridges between the two functional domains is disrupted, and the disruption propagates into the substrate binding domain and opens the α-helical "lidlike" subdomain that partially covers the deep peptide binding channel (*9*, *39*). The resultant chaperone molecule with the lid in the "open" position is the low-affinity state of DnaK (E**−ATP), because in the open position substrates, such as peptides or unfolded segments of proteins, can rapidly enter or rapidly exit the channel (*10*). The subsequent hydrolysis of ATP reestablishes the contacts between the two domains and "closes" the lid, yielding the high-affinity state of DnaK [E−ADP(P_i)], which is likely to have a substrate trapped in the deep channel. Thus, free energy from ATP binding and hydrolysis is harnessed by the chaperone to drive lid opening and closing.

APPENDIX

Considering ADP dissociation from DnaK according to Scheme 3, we describe below the derivation of an expression for the dependence of the observed rate constant for ADP dissociation (k_{obs}) on the parameters $K_d(P_i)$, k_{ADP}, and k^*_{ADP}. The dissociation of ADP from E−ADP(P_i) and E−ADP complexes yields E(P_i) and E species, respectively. We assume that excess ATP instantaneously binds to these two species, yielding the spectroscopically indistinguishable species E**−ATP(P_i) and E**−ATP, respectively. For simplicity, these latter two species are denoted as E**. Thus, the rate of E** formation in Scheme 3 is given by

$$d[E^{**}]/dt = k_{ADP}[E-ADP] + k^*_{ADP}[E-ADP(P_i)] \quad (7)$$

Assuming a rapid equilibrium between E−ADP and E−ADP(P_i), the expression for the equilibrium dissociation constant for P_i dissociation from E−ADP(P_i) complexes [$K_d(P_i) = [P_i]\,[E-ADP]/[E-ADP(P_i)]$] was used to substitute for the [E−ADP(P_i)] term in eq 7, to yield

$$d[E^{**}]/dt = k_{ADP}[E-ADP] + \frac{k^*_{ADP}\,[P_i][E-ADP]}{K_d(P_i)} \quad (8)$$

The mass balance equation ($E_{total} = [E-ADP] + [E-ADP(P_i)] + [E^{**}]$) and the expression for $K_d(P_i)$ were then used to eliminate the term [E−ADP]:

$$d[E^{**}]/dt = \left(k_{ADP} + \frac{k_{ADP}[P_i]}{K_d(P_i)}\right)\left(\frac{K_d(P_i)}{K_d(P_i) + [P_i]}\right)(E_{total} - [E^{**}]) \quad (9)$$

The above equation simplifies to

$$d[E^{**}]/dt = \frac{k_{ADP}K_d(P_i) + k^*_{ADP}\,[P_i]}{K_d(P_i) + [P_i]}(E_{total} - [E^{**}]) \quad (10)$$

thus the observed rate constant for E** formation, or ADP dissociation, is given by

$$k_{obs} = \frac{k_{ADP}K_d(P_i) + k^*_{ADP}\,[P_i]}{K_d(P_i) + [P_i]} \quad (11)$$

Note that when $[P_i] = 0$, $k_{obs} = k_{ADP}$, and when $[P_i] \gg K_d(P_i)$, $k_{obs} = k^*_{ADP}$. The reciprocal of eq 11 is the same as eq 5.

REFERENCES

1. Zylicz, M., LeBowitz, J. H., McMacken, R., and Georgopoulos, C. (1983) *Proc. Natl. Acad. Sci. U.S.A. 80*, 6431−6435.
2. Palleros, D. R., Reid, K. L., Shi, L., Welch, W. J., and Fink, A. L. (1993) *Nature 365*, 664−666.
3. O'Brien, M. C., and McKay, D. B. (1995) *J. Biol. Chem. 270*, 2247−2250.
4. Georgopoulos, C., and Welch, W. J. (1993) *Annu. Rev. Cell Biol. 9*, 601−634.
5. Hendrick, J. P., and Hartl, F.-U. (1993) *Annu. Rev. Biochem. 62*, 349−384.
6. Becker, G., and Craig, E. A. (1994) *Eur. J. Biochem. 219*, 11−23.
7. Flaherty, K. M., DeLuca-Flaherty, C., and McKay, D. B. (1990) *Nature 346*, 623−628.
8. Morshauser, R. C., Wang, H., Glynn, G. C., and Zuiderweg, R. P. (1995) *Biochemistry 34*, 6261−6266.
9. Zhu, X., Zhao, X., Burkholder, W. F., Gragerov, A., Ogata, C. M., Gottesman, M. E., and Hendrickson, W. A. (1996) *Science 272*, 1606−1614.
10. Schmid, D., Baici, A., Gehring, H., and Christen, P. (1994) *Science 263*, 971−973.
11. Prasad, K., Heuser, J., Eisenberg, E., and Greene, L. (1994) *J. Biol. Chem. 269*, 6931−6939.
12. Wilbanks, S. M., Chen, L., Tsuruta, H., Hodgson, K. O., and McKay, D. B. (1995) *Biochemistry 34*, 12095−12106.
13. Shi, L., Kataoka, M., and Fink, A. L. (1996) *Biochemistry 35*, 3297−3308.
14. Banecki, B., Zylicz, M., Bertoli, E., and Tanfani, F. (1992) *J. Biol. Chem. 267*, 25051−25058.
15. Palleros, D. R., Reid, K. L., McCarty, J. S., Walker, G. C., and Fink, A. L. (1992) *J. Biol. Chem. 267*, 5279−5285.
16. Ha, J.-H., and McKay, D. B. (1995) *Biochemistry 34*, 11635−11644.

17. Liberek, K., Skowyra, D., Zylicz, M., Johnson, C., and Georgopoulos, C. (1991) *J. Biol. Chem. 266*, 14491−14496.
18. Buchberger, A., Theyssen, H., Schroder, H., McCarty, J. S., Virgallita, G., Milkereit, P., Reinstein, J., and Bukau, B. (1995) *J. Biol. Chem. 270*, 16903−16910.
19. Fung, K. L., Hilgenberg, L., Wang, N. M., and Chirico, W. J. (1996) *J. Biol. Chem. 271*, 21559−21565.
20. Banecki, B., and Zylicz, M. (1996) *J. Biol. Chem. 271*, 6137−6143.
21. Theyssen, H., Schuster, H.-P., Packschies, L., Bukau, B., and Reinstein, J. (1996) *J. Mol. Biol. 263*, 657−670.
22. Farr, C. D., Galiano, F. J., and Witt, S. N. (1995) *Biochemistry 34*, 15574−15582.
23. Montgomery, D., Jordan, R., McMacken, R., and Freire, E. (1993) *J. Mol. Biol. 232*, 680−692.
24. Chaykin, S. (1966) in *Biochemistry Laboratory Techniques*, p 137, John Wiley & Sons, Inc., New York.
25. Bevington, P. R. (1969) *Data Reduction and Error Analysis for the Physical Sciences*, McGraw-Hill, New York.
26. Bardwell, J. C. A., and Craig, E. A. (1984) *Proc. Natl. Acad. Sci. U.S.A. 81*, 848−852.
27. McCarty, J. S., and Walker, G. C. (1991) *Proc. Natl. Acad. Sci. U.S.A. 88*, 9513−9517.
28. Palleros, D. R., Reid, K. L., Shi, L., and Fink, A. L. (1993) *FEBS Lett. 336*, 124−128.
29. Trybus, K. M., and Taylor, E. W. (1982) *Biochemistry 21*, 1284−1294.
30. Gao, B., Emoto, Y., Greene, L., and Eisenberg, E. (1993) *J. Biol. Chem. 268*, 8507−8513.
31. Burkholder, W. F., Panagiotidis, C. A., Silverstein, S. J., Cegielska, A., Gottesman, M. E., and Gaitanaris, G. A. (1994) *J. Mol. Biol. 242*, 364−377.
32. Ha, J.-H., and McKay, D. B. (1994) *Biochemistry 33*, 14625−14635.
33. Johnson, K. A., and Taylor, E. W. (1978) *Biochemistry 17*, 3432−3442.
34. Hiromi, K. (1979) *Kinetics of Fast Enzyme Reactions. Theory and Practice*, John Wiley & Sons, New York.
35. Hoggett, J. G., and Kellett, G. L. (1995) *Biochem. J. 305*, 405−410.
36. Anderson, C. M., Stenkamp, R. E., McDonald, R. C., and Steitz, T. A. (1978) *J. Mol. Biol. 123*, 207−219.
37. Flaherty, K. M., Wilbanks, S. M., DeLuca-Flaherty, C., and McKay, D. B. (1994) *J. Biol. Chem. 269*, 12899−12907.
38. McCarty, J. S., Buchberger, A., Reinstein, J., and Bukau, B. (1995) *J. Mol. Biol. 249*, 126−137.
39. Gething, M.-J. (1996) *Curr. Biol. 6*, 1573−1576.

BI9720484